Wind or Hydro Homo-Heteropolar Synchronous Generators: Equivalent Magnetic Circuit and FEM Analysis

Sorin Ioan Deaconu1,, Marcel Topor1, Lucian Nicolae Tutelea2, Ilie Nucă3, and Marcel Burduniuc3*

[1]Electrical Engineering and Industrial Informatics Department, Politehnica University, Timisoara, Romania
[2]Electrical Engineering Department, Politehnica University, Timisoara, Romania
[3]Department of Electrical Engineering, Technical University of Moldova, Chişinău, Republic of Moldova

Abstract. In an effort to introduce a low cost (PM less), low power electric wind or hydro generators, this paper reports on preliminary design aspects, equivalent magnetic circuit and 3D FEM analysis of a 2.5 KVA, 250-1000 rpm, reactive homo-heteropolar brushless synchronous machine (RHHBSM).

1 Introduction

One of the main disadvantages of the classic synchronous machines is the armature's excitation winding which determines a great rotor weight and inertia and involves the sliding contacts' existence (brushes and slips rings). Reference [1] presented a new form of heteropolar linear synchronous machine that is capable of providing both thrust and lifting force at relatively high efficiencies and power factor. In [2] is presented a rotary reactive homopolar synchronous machine with stator excitation which removes the disadvantages of the classic synchronous machines.

Conception constraints on electro-technical devices require numerical simulations to be as close as possible to its actual operating conditions. Then, it is necessary to have coupled physical models of devices, especially, for electrical, magnetic and mechanical coupled models which allow the simulation of loaded rotating machines [3].

Finite elements method (F.E.M.) allows such coupling for 2D plan modeling devices. Nevertheless, it requires a lot of calculation time. Its use for three dimensional typical machine has never been done until nowadays and calculation time will be even longer [4].

In order to obtain the best results in designing of the special electric machines, it should be used both the classic methods and the numerical calculation methods. The calculation should be based on a mathematic model as accurate possible. Based on this model are determined by simulation the characteristics of the machine in non-saturated and saturated regime [2], [5].

The designing particularities of these types of generators are linked to the axial character of the magnetic field distribution. The field calculation in the machine can be achieved by the finite elements method [6], or by field tubes method [2], [5], [7-10]. Taking into consideration the axial distribution of the machine field, it is necessary a three-dimensional modeling of the machine field. For this three-dimensional model is required a specialized software that needs a performance computer, and the calculations time could be high.

2 The constructive elements

The reactive homopolar (RHBSM) and homo-heteropolar brushless synchronous machines (RHHBSM) which we'll analyze further are rotary machines. In order to understand their constructive elements, in Fig.1 is presenting a longitudinal section. The excitation coil has a ring shape and is placed in the windows of the U or E-shaped laminations stack (Fig. 1 a, b), and, at passing of the rotor poles, the field is closing, having by this a rectangular variation form. When the rotor pole is not under the laminations stack, the field is practically null.

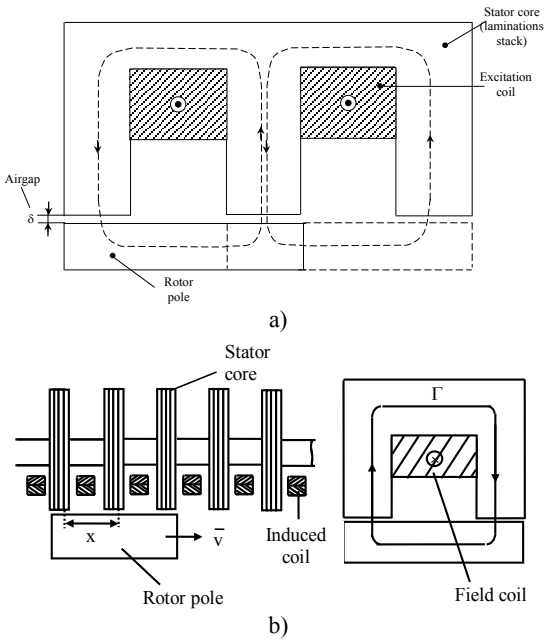

Fig. 1. Longitudinal magnetic circuit section in: a) homo-heteropolar synchronous machine; b) homopolar synchronous machine.

* sorin.deaconu@fih.upt.ro

The constructive elements of the novel RHBSM and RHHBSM, are presented in Fig. 2, 3 and 4 in a 3D and 2D view.

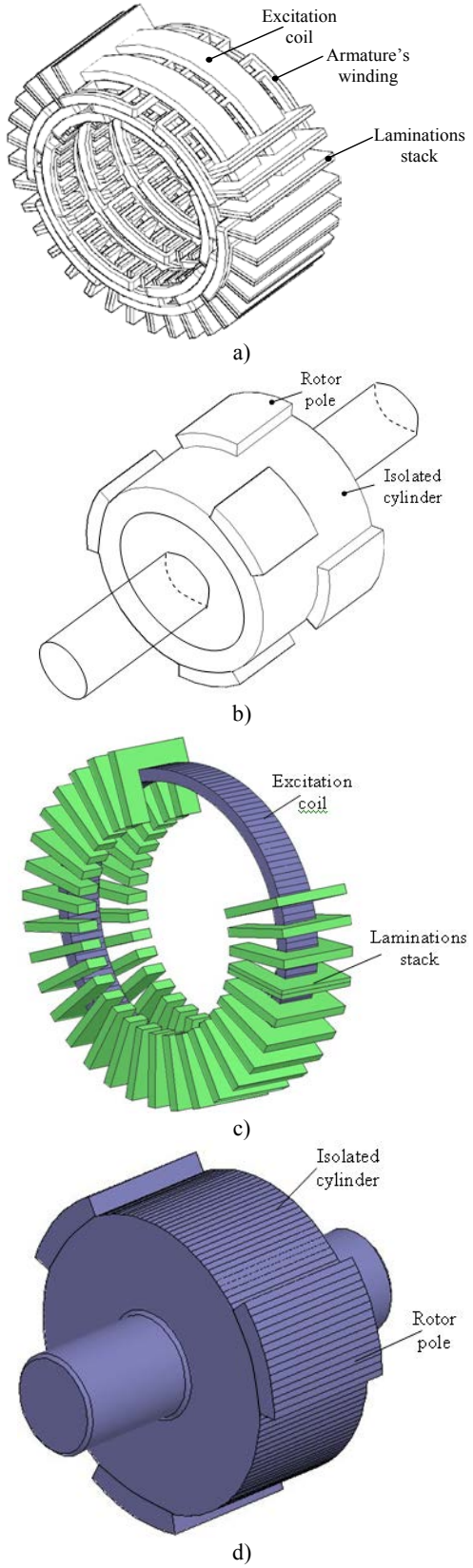

Fig. 2. a) 3D representation of stator magnetic circuit with excitation and phase winding coils of RHHBSM; b) 3D representation of the rotor of RHHBSM; c) 3D representation of the stator magnetic circuit with excitation coil of RHBSM; d) 3D representation of the rotor of RHBSM.

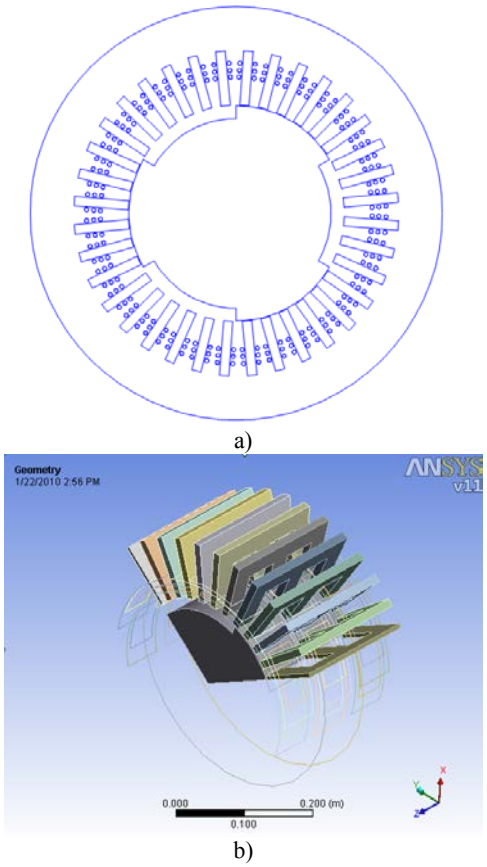

Fig. 3. RHHBSM: a) 2D representation of stator and rotor magnetic circuit, with armature phase winding coils. b) 3D geometry representation.

The excitation coils has a ring shape and are placed in the windows of the E-shaped laminations stack. The armature AC winding is placed in the open slots, formed between the pockets of lamination stack. To design the three dimensional magnetic structure of the RHHBSM is necessary to identify the flux distribution of the machine. The geometry of the RHHBSM poses a challenging problem because of the various cross-couplings between the rotor and stator. The flux distribution caused by the AC winding and by the DC excitation is investigated separately.

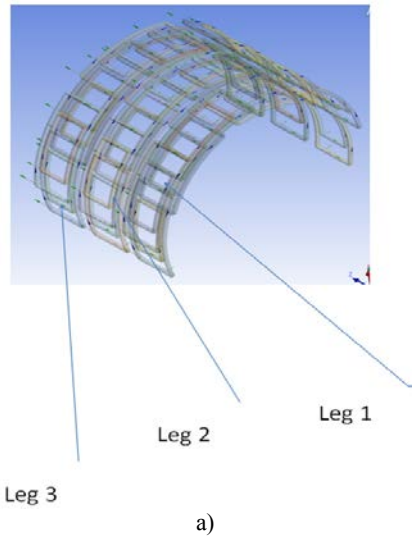

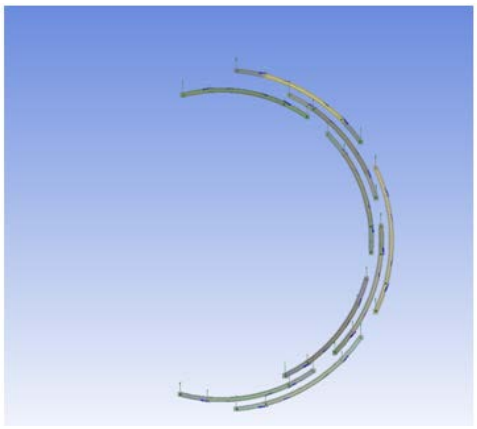

b)

Fig. 4. a) 3D representation of stator winding coils: a) for three legs; b) the winding from one leg (leg 1) for all three phases which is placed in hree layers.

3 The method of equivalent magnetic circuits

A quasi-stationary magnetic field can be divided in field tubes, which are geometrical figures in which all the field lines are perpendicular on its bases and do not intersect the side surface. The plans of the same scalar magnetic potential are perpendicular on the flux lines. Is noted with Γ the specific permeance on the length unit, with λ the permeance, with μ_0 ($\mu_0 = 4\pi \cdot 10^{-7}$ H/m) the void's magnetic permeability and with l the active conductor's length in the slot:

$$\Gamma = \frac{\lambda}{\mu_0 \cdot l}. \quad (1)$$

In fig. 5 is presenting a conductor into an elementary slot where were made the notations: h the slot depth, w the slot opening towards the air-gap, I the current that circulates through the conductor from the slot, ϕ the magnetic flux produced by the current that circulates through the conductor and dy the distance element by axis y.

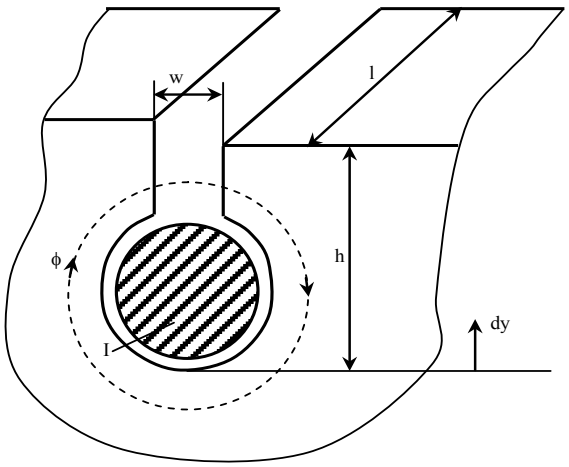

Fig. 5. Elementary slot based on which is calculated the specific permeance.

The flux element, where B is the magnetic induction in the slot, dA the area element and H the magnetic field's intensity, has the expression:

$$d\phi = B \cdot dA = B \cdot l \cdot dy = \mu_0 \cdot H \cdot l \cdot dy . \quad (2)$$

If is neglected the magnetic voltage drop in the iron core comparatively with w from the slot, from the magnetic circuit's law is deduced:

$$H \cdot w = I = U_H , \quad (3)$$

$$d\phi = \mu_0 \cdot \frac{I}{w} \cdot l \cdot dy . \quad (4)$$

By integration is obtained:

$$\phi = \int_0^h d\phi = \mu_0 \cdot \frac{I}{w} \cdot l \cdot h . \quad (5)$$

Is calculated the magnetic reluctance R_m and then the specific permeance Γ:

$$R_m = \frac{U_H}{\phi} = \frac{I}{\phi} = \frac{w}{\mu_0 \cdot l \cdot h} , \quad (6)$$

$$\lambda = \frac{1}{R_m} = \frac{\mu_0 \cdot l \cdot h}{w} , \quad (7)$$

$$\Gamma = \frac{h}{w} . \quad (8)$$

Based on these premises, considering the configuration of the RHBSM or RHHBSM, presented in fig. 1, where $\lambda_{i,j}$ is the permeance between the stator tooth i and the rotor pole j depending on angle ϑ between the axis of stator tooth i and the axis of the rotor pole j, the permeance in the air-gap has the expression [3]:

$$\lambda_{i,j}(\vartheta) = \lambda_{max} \cdot b(\vartheta) . \quad (9)$$

If D_{si} is the inner stator diameter and D_{r0} the outer rotor diameter, the term b(ϑ) has the definition relation [11-15]:

$$b(\vartheta) = \frac{b'(\vartheta) - b'(\pi)}{b'(0) - b'(\pi)} \qquad -\pi \le \vartheta \le \pi , \quad (10)$$

$$\beta = ln\frac{D_{si}}{D_{r0}} , \quad (11)$$

$$b'(\vartheta) = ln\frac{cosh\left(\pi \cdot \frac{\vartheta - \vartheta_t}{2\beta}\right) \cdot cosh\left(\pi \cdot \frac{\vartheta + \vartheta_t}{2\beta}\right)}{cosh^2\left(\pi \cdot \frac{\vartheta}{2\beta}\right)} - \frac{\vartheta_t^2}{2\beta} + \\ + 4\sum_{k=1}^{\infty} \frac{e^{-\left(k \cdot \frac{\pi}{\beta}\right)}}{sinh\left(k \cdot \frac{\pi^2}{\beta}\right)} \cdot cosh\left(k \cdot \pi \cdot \frac{\vartheta}{\beta}\right) \cdot \left[cosh\left(k \cdot \pi \cdot \frac{\vartheta_t}{\beta}\right) - 1\right]. \quad (12)$$

The graphic representation of b(ϑ) is given in fig. 6.

In fig. 7 is presenting the permeance's variation form in the air-gap, with the previous specifications.

Because the number of stator slots and the number of rotor poles differ, w_{st} being the width towards the air-gap of the stator tooth, w_{rt} the width towards the air-gap of the rotor pole and δ the air-gap, the term λ_{max} has the expression:

$$\lambda_{max} = \mu_0 \cdot \frac{l \cdot w_{min}}{\delta}, \quad (13)$$

$$w_{min} = min\left(w_{st}, w_{rt}\right). \quad (14)$$

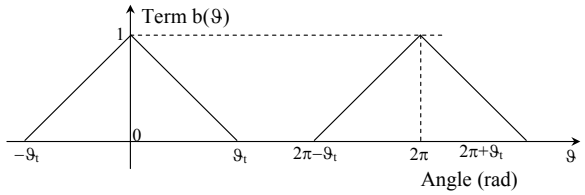

Fig. 6. Variation form of the term b(ϑ).

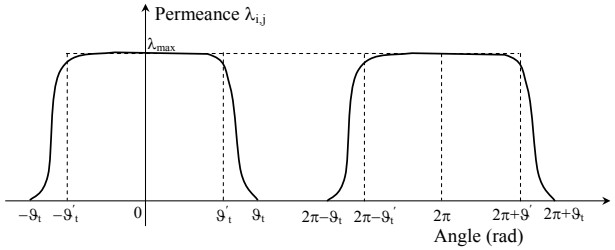

Fig. 7. Variation form of permeance in air-gap.

If D_{ag} is the average diameter in the air-gap, are defined the terms [3]:

$$\vartheta_t' = \frac{\left|w_{st} - w_{rt}\right|}{D_{ag}}, \quad (15)$$

θ_{ss} the width of stator slot the towards the air-gap, θ_{sr} the width of the interpolar space between two rotor poles and

$$\vartheta_t = \frac{w_{st} + w_{rt} + \theta_{ss} + \theta_{sr}}{D_{ag}}, \quad (16)$$

where

$$D_{ag} = \frac{D_{si} + D_{r0}}{2}. \quad (17)$$

From the anterior relations, by replacement results:

$$\lambda_{i,j} = \begin{cases} \lambda_{max} & 0 \le \vartheta \le \vartheta_t' \text{ and } 2\pi - \vartheta_t' \le \vartheta \le 2\pi + \vartheta_t' \\ \lambda_{max} \cdot \dfrac{1 + \cos\pi \dfrac{\vartheta - \vartheta_t'}{\vartheta_t - \vartheta_t'}}{2} & \vartheta_t' \le \vartheta \le \vartheta_t \\ \lambda_{max} \cdot \dfrac{1 + \cos\pi \dfrac{\vartheta - 2\pi + \vartheta_t'}{\vartheta_t - \vartheta_t'}}{2} & 2\pi - \vartheta_t \le \vartheta \le 2\pi - \vartheta_t' \\ 0 & \vartheta_t \le \vartheta \le 2\pi - \vartheta_t. \end{cases} \quad (18)$$

To define the mathematical model's equations, is started from the magnetic circuit's shape with open slots, between the adjacent pockets of laminates. In fig. 8 is presenting the stator slot in which are placed two sides of the coil passed-through by the currents i_u and i_l and which have the number of windings w_u and w_l. The number of stator pockets is noted with k and the number of rotor poles with l.

By means of the equivalent magnetic circuits method [11-15] is deduced the equivalent diagram of the magnetic circuit which is presented in fig. 9 [3].

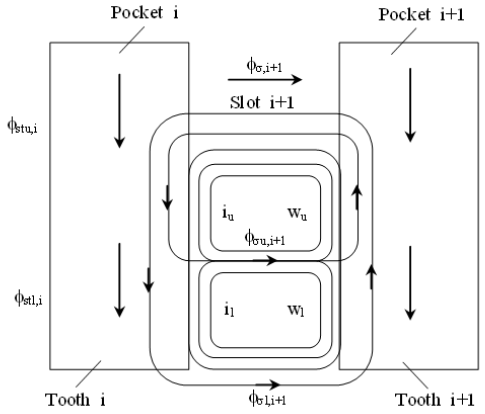

Fig. 8. Stator slot with the armature's winding.

In fig. 9 were made the following notations: $R_{s\sigma a}$ – the reluctance of the slot's superior part, $R_{s\sigma u}$ – the reluctance of the stator slot's median part, $R_{s\sigma l}$ – the reluctance of the stator slot's inferior part, R_{stu} and R_{stl} – the superior and inferior reluctances of the stator teeth, ϕ - the fluxes through air or core in different areas, V_m – the magnetic potential and θ - the magnetomotive force. By composing and equivalence is obtained a simplified equivalent diagram presented in fig. 10. The binding relations between the quantities from fig. 10 and the ones from fig. 9 are:

$$R_{s\sigma} = R_{s\sigma u} + R_{s\sigma l}, \quad (19)$$

$$R_{st,i} = R_{stu,i} + R_{stl,i}, \quad (20)$$

$$\phi_{st,i} = \phi_{stu,i} + \phi_{stl,i}, \quad (21)$$

$$\theta_{st,i} = \theta_{stu,i} + \theta_{stl,i}, \quad (22)$$

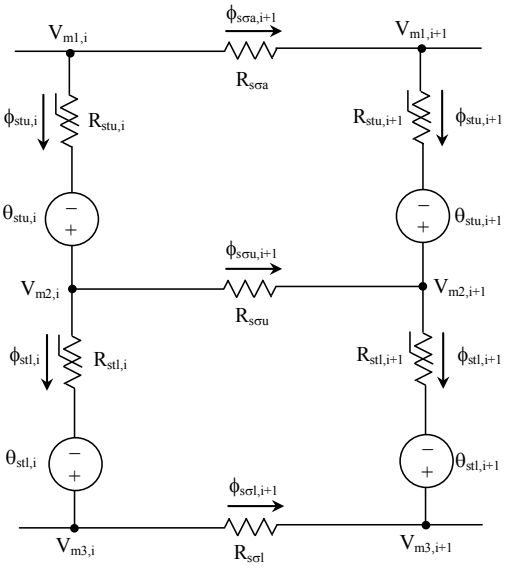

Fig. 9. The equivalent diagram of the transversal magnetic circuit for a slot.

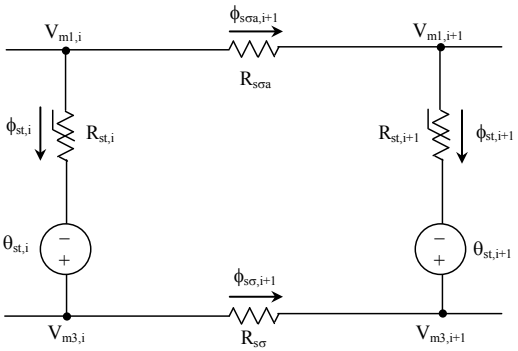

Fig. 10. The simplified equivalent diagram of the transversal magnetic circuit for a slot.

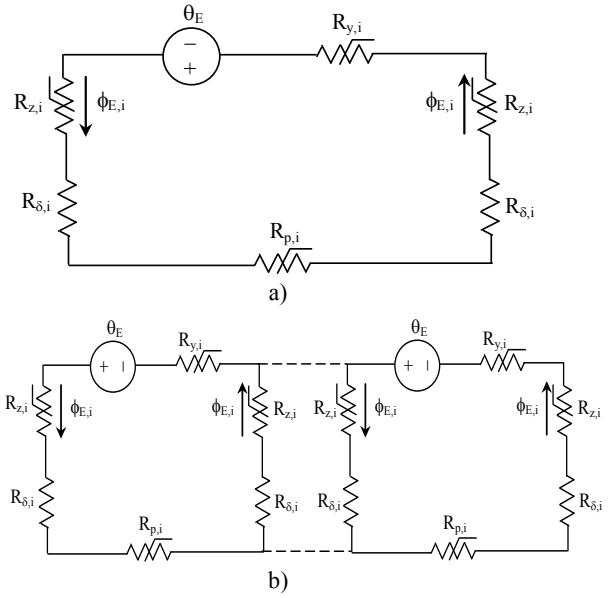

Fig. 11. Equivalent diagram of the longitudinal magnetic circuit of a pocket of laminations.

For the E or the U-shaped magnetic circuit of the stator pockets of laminates (fig. 1), the equivalent magnetic circuits are presented in fig. 11 a and fig. 11 b, where R_y is the yoke's reluctance, R_z the column's reluctance, R_δ the air-gap's reluctance, R_p the reluctance of the pole under the pocket of laminates and θ_E the source of magnetomotive force due to excitation. The index i refers to the number of the stator pocket of laminates. Solving of the equivalent magnetic circuits is made by determining the magnetic scalar fluxes and potentials in all nodes [11], for given ampere-turns and known permeances. Based on the duality between the electric field and magnetic field, a magnetic circuit contains elements with a unique value of the magnetization curve and it can be equalized with a dry-current electric circuit with linear or non-linear sources and resistances. If the non-linear reluctances have their magnetization curve strictly monotonous and increasing, then, for a set of initial conditions there is a unique solution if the hysteresis is neglected.

In fig. 12 is presenting the equivalent diagram of the magnetic circuit considering an ampere-turns of equivalent reaction θ_1 for the armature's winding. The values of permeances, fluxes and ampere-turns from fig. 12 have the expressions (23), (24) and (25) [3], where μ_{Fe} and μ_0 are the magnetic permeabilities of the iron core and air, S_{Fe} and S_a the sections, $l_m/2$ the field line's length, λ_{rFe} the rotor iron permeance under a pocket of laminates beneath which has entered the rotor pole to a central angle $\vartheta_i - \vartheta$ (ϑ_i is the central angle corresponding to a pocket of laminates beneath which has not entered the rotor pole), λ_{ra} the air's rotor permeance under a pocket of laminates corresponding to the central angle ϑ, λ_r the rotor equivalent permeance under a pocket of laminates.

$$\lambda_{rFe} = \mu_{Fe} \cdot \frac{S_{Fe}}{l_m / 2}, \quad (23)$$

$$\lambda_{ra} = \mu_0 \cdot \frac{S_a}{l_m / 2}, \quad (24)$$

$$\lambda_r = \frac{\mu_{Fe} \cdot S_{Fe} + \mu_0 \cdot S_a}{l_m / 2}. \quad (25)$$

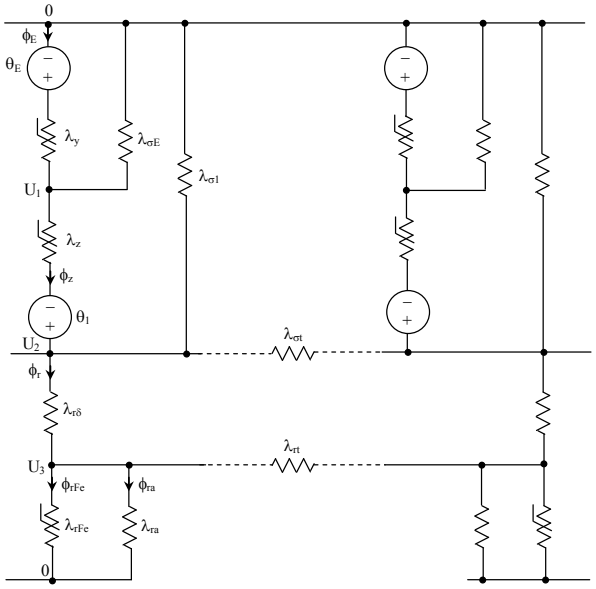

Fig. 12. The equivalent diagram of magnetic circuit with a equivalent ampere-turns for armature winding

4 3D FEM analysis

The finite element method is used in order to obtain key parameters of the RHHBSM. Since the topology of the machine has is a purely 3 dimensional flux paths one the complete transient characteristics and parameters can not be obtained without an extensive computation effort. Finite element analysis of the machine was done a commercial software platform. When applied to electrical machines, the described problem is usually reduced to cover only one pole or one pole pair with the help of boundary and symmetry conditions in order to reduce the computation time. The windings are in star connections and thus the excitation current shares among phases are $I_A = I$, $I_B = I_C = -I/2$. From the 3D finite element we will consider only some key values or verification values which can not be obtained from other means. Since this topology has a 3D field the model required and 3D magnetostatic model solver. In order to simplify

the solution we have used only one third model (Fig. 13-17) taking advantage of the machine symmetry. Using the 3D FEM tool is still time-consuming, which limits its use in parameter investigation process.

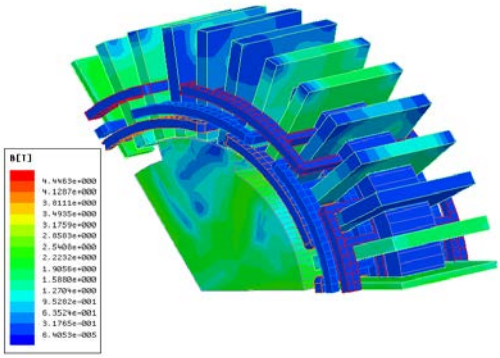

a)

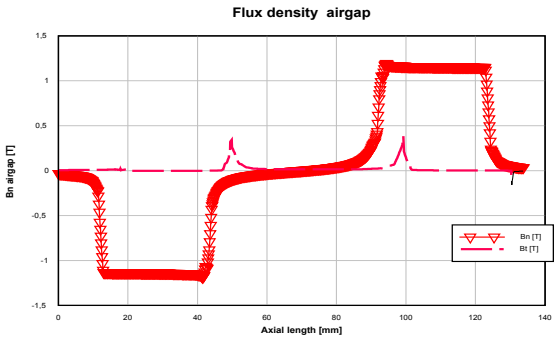

b)

Fig. 13. Finite element results for homopolar case: a) 3D field; b) airgap flux density for Ie=6A at no load.

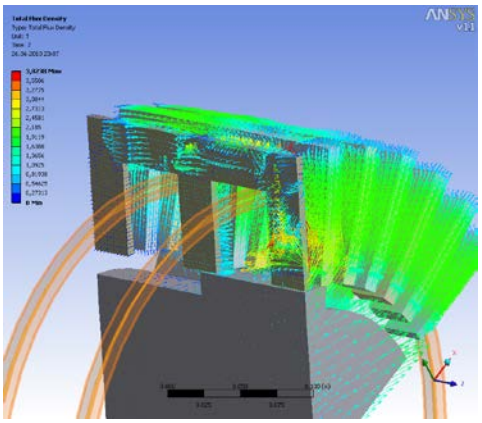

a)

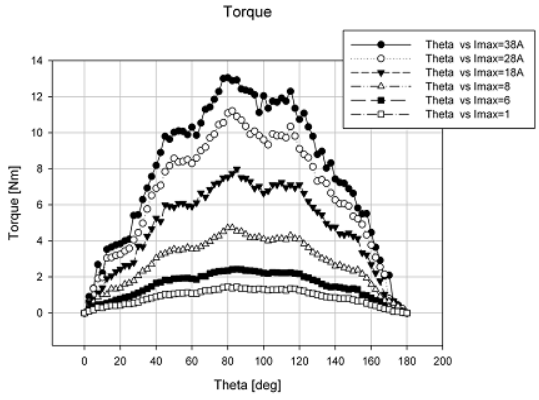

b)

Fig. 14. Finite element results for heteropolar case: a) 3D field; b) torque versus angle at different currents.

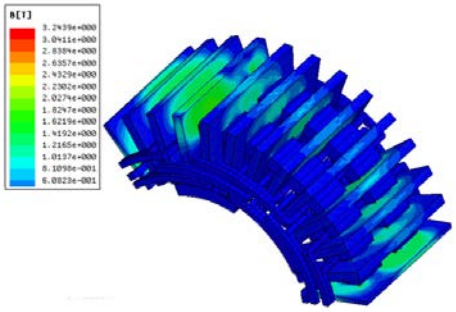

Fig. 15. Finite element results for heteropolar case: 3D field.

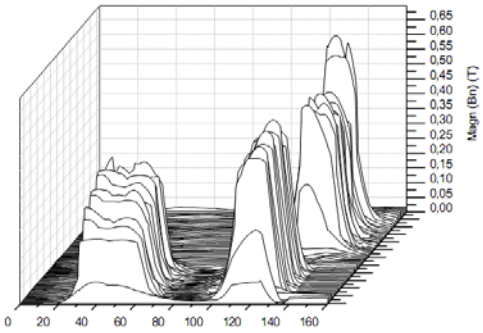

Fig. 16. Finite element results for heteropolar case: airgap flux density.

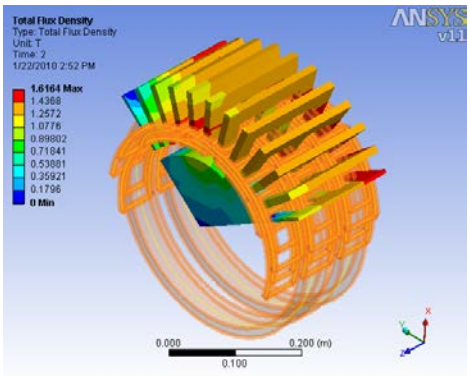

Fig. 17. Finite element results for heteropolar case: total flux density at $I_a=I_b=I_c=0$ and $I_{exc}=I_{excN}$.

The solution of the finite element model using a 3D finite element solver took about 6 hours per step. The airgap flux density magnitude (the absolute value of B) is presented in Fig 16. Inductance evaluation from finite element solution shows that the machine is not saturated since the maximum airgap value is below 1T. The static torque produced by constant currents and varying the position is presented in Fig. 11 from this value the maximum torque can be obtained equal to 11 (Nm).

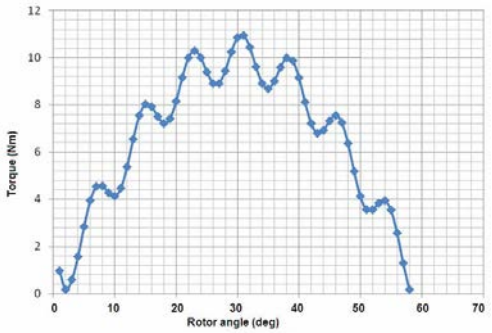

Fig. 18. Static torque variation with position obtained from 3D FEM currents are constant and only the position is varied.

5 Conclusions

The main advantage of the RHBSM and RHHBSM are their improved capability to operate at variable speed for wind or hydro power plants. The design method was validated also by means of 3D FEM model. General performance characteristics of ampere-turns, inductor flux, resulting flux and torque variation are presented.

References

1. S.I. Deaconu, L.N. Tutelea, G.N. Popa, I. Popa and C. Abrudean, *Optimizing the Designing of a Reactive Homopolar Synchronous Machine with Stator Excitation*, IECON 2008, 34th Annual Conference of the IEEE Industrial Electronics Society, Orlando, Florida, USA, 10-12 November, pp. 1311-1318, (2008)
2. S.I. Deaconu, M. Topor, L.N. Tutelea, G.N. Popa and C. Abrudean, *Mathematical Model of a Reactive Homopolar Synchronous Machine with Stator Excitation*, EPE-PEMC 2009, Barcelona, Spain, 8-10 September, pp. 2269-2277, (2009)
3. S.I. Deaconu, M. Topor, L.N. Tutelea, G.N. Popa and C. Abrudean, *Modeling and Experimental Investigations of a Reactive Homo-Heteropolar Brushless Synchronous Machine*, IECON 2009, *35th* Annual Conference of the IEEE Industrial Electronics Society, Porto, Portugal, USA, 3-5 November, pp. 1209-1216, (2009)
4. M.J. Balchim, and J.F. Eastham, *Characteristics of heteropolar linear synchronous machine with passive secondary*, Electric Power Application, **vol. 2**, no. 8, pp. 213-218, December (1979)
5. J. He and F. Lin, *A high frequency high power IGBT inverter drive for 45 HP/16.000 RPM brushless homopolar inductor motor*, Conference Record of the IEEE IAS Annual Meeting, pp. 9-15, (1995)
6. M. Siegl and V. Kotrba, *Losses and cooling of a high-output power homopolar alternator*, IEEE Fifth International Conference on electrical Machine and Drives (Conf. Publ. No. 341), London, U.K., 11-13 Sept., pp. 295-299, (1991)
7. G. P. Rao, J. L. Kirtby, D. C. Meeker Jr. and K. J. Donegan, *Hybrid permanent magnet/homopolar generator and motor*, U. S. Patent 6097124, Aug. 1, (2000)
8. O. Ichikawa, A. Chiba and T. Fukao, *Development of Homo-Polar Type of Bearingless Motors*, Conference Record of the 1999 IEEE IAS Annual Meeting, pp. 1223-1228, (1999)
9. M. Hippner and R. G. Harley, *High speed synchronous homopolar and permanent magnet machines comparative study*, Conference Record of the IEEE IAS Annual Meeting, pp. 74-78, (1992)
10. H. Hofman and S. R. Sanders, *High speed synchronous machine with minimized rotor losses*, IEEE Transactions on Industry Applications, vol. 36, no. 2, Mar., pp. 531-539, (2000)
11. P. Tsao, M. Senesky and S. Sanders, A Synchronous Homopolar Machine for High-Speed Applications, Conference Record of IEEE IAS Annual Meeting, pp. 406-416, (2002)
12. L. Vido, M. Gabsi, M. Lecrivain, Y. Amara and F. Chabot, *Homopolar and Bipolar Hybrid Excitation Synchronous Machine*, IEEE Transactions on Energy Conversion, **vol. 21**, no. 3, September, pp 1212-1218, (2006)
13. S.I. Deaconu, *The study of control brushless electrical generator*, PHD Thesis (in Romanian), Politechnica University of Timisoara, Romania, unpublished, (1998)
14. I. Boldea and S.A. Nasar, *Electric drives*, 2nd edition, CRC Press, Taylor and Francis Group, pp. 256-375, New York, (2005)
15. A. Kelemen, M. Imecs, *Field-Oriented Control of AC Machines* (in Romanian), Academic Publishing House, pp. 136-240, ISBN 973-27-0032-7, Bucuresti, Romania, (1989)